Published by :
http://www.ijert.org

International Journal of Engineering Research & Technology (IJERT)
ISSN: 2278-0181
Volume 13, Issue 03 March 2024

Modelling the Performance of Halo Impact Protection Device of F1 Race Cars

Abhishek Cherukara
School of Engineering
Newcastle University
Newcastle upon Tyne, NE1 7RU,
United Kingdom.

Hemantha Kumar Yeddu
Department of Mechanical Engineering,
Lappeenranta University of Technology (LUT)
Lappeenranta,
53850 Finland.

***Abstract*— The macroscale performance of halo impact protection device, made of Ti-6Al- 4V alloy, used in F1 race cars is studied using finite element (FE) simulations. The halo and its components are designed based on FiA (F´ed´eration Internationale de l'Automobile) standards. The halo is studied under static and dynamic loading conditions. The dynamic impact loading analysis is performed by considering a real-life F1 accident scenario, i.e., impact of moving halo at a high speed against a steel barrier. The dynamic impact of the halo is studied by considering the Johnson-Cook constitutive model and the input mechanical properties are considered based on the different phases present in the material during the impact. The static loading analysis shows that the device is safe and adheres to FiA standards. The dynamic impact loading analysis shows that the device fails and shows the regions of high stress, plastic strain, and damage in the halo. The simulations emphasize the importance of weld joints in deciding the safety of the halo device of F1 race cars.**

***Keywords*— Finite element simulations, titanium alloy, impact loading, Johnson-Cook constitutive model, F1 Race cars**

I. INTRODUCTION

Formula 1 (F1) is often regarded as the pinnacle of motor sport, although the risk of injuries and fatalities is very high. The safety of F1 drivers is less compromised in recent times, mainly due to the series of safety innovations added to a F1 car. One such safety innovation, introduced by the FiA (F´ed´eration Internationale de l'Automobile) after the death of a race car driver due to head injury, was the Halo impact protection system that protects the drivers from severe head injuries and death [1]. The addition of the halo protection device has shown to improve the driver's survival rate by 17% [2]. The Bahrain Grand Prix in 2020 justified the relevance of the halo in F1 as one of the drivers, Romain Grosjean's race car collided with a stationary barrier that split open as the car passed through it at approximately 140 miles per hour. The driver survived miraculously, mainly due to the halo impact protection system [3]. The addition of halo was further emphasized during the 2022 Great British Grand Prix when Zhou Guanyu's car glided across the track upside down on the halo and into the gravel and finally stopped by the catch fencing, however without any major injuries to the driver [4].

The performance of the halo during crash must be studied to understand its behaviour under dynamic loading, which can aid in improving the design of the halo. In addition, the performance of halo under static loading should also be studied to ensure that the design of halo is acceptable according to FiA standards [5,6]. Finite element analysis (FEA) can provide insights into the macroscale performance of the halo under different loading conditions [7]. However, the crash behaviour of the halo has not been analysed using FEA by considering realistic dynamic loading conditions and accurate material properties as well as material models.

Grade 5 Titanium, i.e., Ti-6Al-4V alloy, has been selected as the material for the halo after extensive research and testing by FiA [8]. Phase transformations can occur in titanium alloys under different thermomechanical conditions and can lead to various phases, viz. α, β and ω. At ambient pressure, Ti-6Al-4V alloy transforms from α to $\alpha + \beta$ at 1070 K and to β at 1280 K [9,10]. α transforms to ω, a brittle phase, at 26–33 GPa in a martensitic manner [9,11,12]. α to ω transformation has also been observed in pure Ti during hydrostatic and non-hydrostatic pressure loading [13,14] as well as during shock loading [14-16].

The formation of highly brittle ω phase during impact loading can affect the mechanical properties of Ti–6Al-4V alloys and consequently the performance of the halo. Therefore, its formation during the impact loading should be accounted for during the stress analysis of the halo to further improve its design and performance. In the present work FEA is performed to analyse the macroscale performance of the halo device under static loading conditions and during the impact of the halo against a steel barrier by considering the mechanical properties affected by different phases, including the omega phase in Ti-6Al-4V alloy.

II. FINITE ELEMENT ANALYSIS

Static and dynamic analyses are performed on the halo device using the finite element analysis. The halo device is assembled using the following components: a central pylon, two tubes that make a U-section and two brackets with circular holes (Fig. 1a). All the components are considered to be made of Ti–6 wt.%Al–4 wt.%V alloy. Based on the FiA standards [5, 6], the components and the assembled halo (Fig. 1a) are designed using Autodesk Inventor [17]. Finite element analysis (FEA) of the halo is performed using ANSYS software [18]. As the components of the halo are usually welded, the joint regions between the components are considered as 'Bonded' in FEA. The pylon is connected to the front part of the vehicle through the hole on the pylon whereas the two rear ends of the tubular 'U' section is attached to the rear of the vehicle by means of the circular holes in the two brackets (Fig. 1a). Frictionless support is considered at these three contact points (holes). As the rear end of the halo is wrapped within the exterior surface of the F1 car, cylindrical support is considered on the two exterior faces

International Journal of Engineering Research & Technology (IJERT)
ISSN: 2278-0181
Volume 13, Issue 03 March 2024

of the brackets so that the brackets possess tangential freedom and constrained in the axial and radial directions. A zero displacement constraint in the X-direction is applied on the bottom face of the pylon to ensure that the halo does not move sideways when forces are applied. The mesh details and the loading conditions are explained in the following sections.

A. Static Analysis

A triangular finite element mesh (Fig. 1b) with an element size of 1 mm is considered in the regions where load is applied on the pylon whereas in the other areas of the pylon an element size of 6 mm is considered. Rectangular finite elements sized 6 mm are considered in the other regions of the halo whereas in the brackets the element size is 3 mm. A resultant force of 125 kN is applied on the front part of the pylon (Fig. 1b) and the resultant von Mises equivalent stress will be compared with the static yield strength of the material to analyse the component's deformation behaviour. Based on FiA's loading specifications [6], this resultant force is composed of 116 kN in the negative Y direction and a force of 46 kN acting in the negative Z direction. In addition, the following loading requirements by FiA were also adhered to: the load must be applied at a position of 190 mm rearward of the front fixing axis and 170 mm above the front fixing axis.

B. Dynamic Analysis

Dynamic analysis of the halo device is performed using the finite element analysis (FEA). The halo device is assembled using the following components: a central pylon, two tubes that make a U-section and two brackets with circular holes (Fig. 1a). All the components are considered to be made of Ti–6 wt.% Al–4 wt. %V alloy. Based on the FiA standards [5, 6], the components and the assembled halo (Fig. 1a) are designed using Autodesk Inventor [17]. FEA of the halo is performed using ANSYS software [18]. As the components of the halo are usually welded, the joint regions between the components are considered to be 'Bonded' in FEA. The pylon is connected to the front part of the vehicle through the hole on the pylon whereas the two rear ends of the tubular 'U' section is attached to the rear of the vehicle by means of the circular holes in the two brackets (Fig. 1a). Frictionless support is considered at these three contact points (holes). As the rear end of the halo is wrapped within the exterior surface of the F1 car, cylindrical support is considered on the two exterior faces of the brackets so that the brackets possess tangential freedom and constrained in the axial and radial directions. A zero displacement constraint in the X-direction is applied on the bottom face of the pylon to ensure that the halo does not move sideways when forces are applied.

The dynamic analysis is performed by considering a real-life accident of the collision of the moving halo against a stationary ARMCO steel barrier [3]. The analysis is performed using explicit dynamics suite in ANSYS and by considering Johnson-Cook (J-C) constitutive model [19–21].

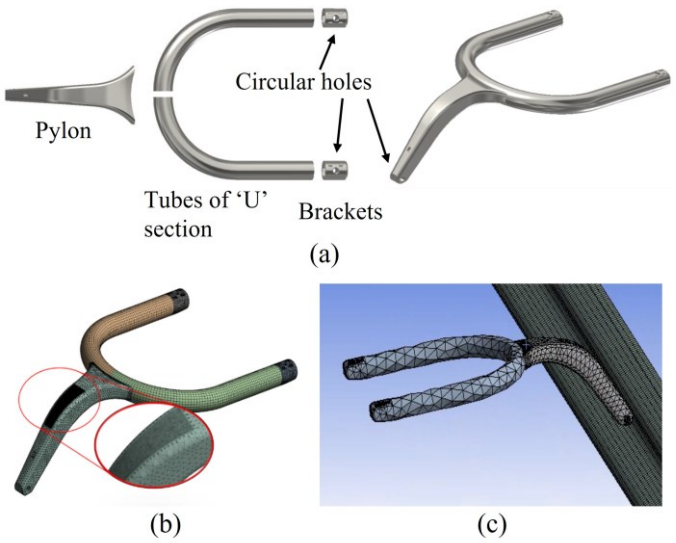

Fig. 1. (a) Components and the final assembly of the halo. Finite element (FE) mesh used in the (b) static loading analysis of the halo and (c) impact loading analysis of the halo against a steel barrier.

J-C strength model is expressed as [19, 20]:

$$\sigma(\varepsilon, \dot{\varepsilon}, T) = (A + B\varepsilon^n)\left(1 + C ln\left(\frac{\dot{\varepsilon}}{\dot{\varepsilon}_{ref}}\right)\right)\left[1 - \left(\frac{T - T_r}{T_m - T_r}\right)^m\right] \quad (1),$$

where σ is the equivalent stress, ε is the equivalent plastic strain, A is the static yield strength, B is hardening modulus, C is strain rate sensitivity coefficient, m is thermal sensitivity coefficient, n is strain hardening coefficient, $\dot{\varepsilon}$ is the strain rate, $\dot{\varepsilon}_{ref}$ is the reference strain rate, T is the deformation temperature, T_r is room temperature and T_m is the melting temperature.

J-C failure model is expressed as [21, 22]:

$$\varepsilon_f = [D_1 + D_2 exp(D_3\eta)]\left[1 + D_4 ln\left(\frac{\dot{\varepsilon}}{\dot{\varepsilon}_{ref}}\right)\right]\left[1 + D_5\left(\frac{T - T_r}{T_m - T_r}\right)\right] \quad (2),$$

where η is stress tri-axiality ratio and $D_1 - D_5$ are material parameters determined from experiments [21]. The input data used in the J-C strength and J-C failure models are shown in Tables 1 and 2, respectively.

TABLE 1 INPUT DATA USED IN J-C STRENGTH MODEL [19].

A (MPa)	B (MPa)	C	n	m	T_m (K)
1030	380	0.042	0.578	0.633	1877

The static yield strength used in the static analysis and dynamic impact loading (A in Eq. (1)) is estimated by considering the phase composition of Ti-6Al-4V alloy after the standard heat treatments [23, 24] and after the α–ω phase transformation due to impact loading. The phase fractions estimated are 15% α, 58% β, 12% α′ and 15% ω [23]. By considering the yield strengths of α, β, α′ and ω as 694 [25], 1073 [26], 1200 [27] and 1075 MPa [28], respectively, the static yield strength (A) of the material is estimated as 1030 MPa (Table 1).

Published by :
http://www.ijert.org

International Journal of Engineering Research & Technology (IJERT)
ISSN: 2278-0181
Volume 13, Issue 03 March 2024

TABLE 2 INPUT DATA USED IN J-C FAILURE MODEL [21].

D_1	D_2	D_3	D_4	D_5
0.01546	1.349	-2.144	0.04323	0.6815

The halo, with a weight of 7 kg (m), attached to the vehicle is considered to be travelling with a velocity (v) of 375 km/hr towards the barrier. Due to computational limitations, only the initial 1.5×10^{-5} s of the collision are considered and the barrier is positioned at a distance (d) of 0.25 mm away from the halo. The impact force of the halo is calculated using $F_{max} = mv^2/2d$ as 151.91 MN.

An adaptive triangular mesh is used in the contact and welded regions of the central pylon of the halo (Fig. 1c). In other areas of the pylon a triangular mesh with element size of 15 mm is used whereas 30 mm element size is considered in the U- section of the halo. The steel barrier with a thickness of 3 mm is constrained using a fixed support, applied to the three faces (top, middle and bottom) of the barrier (Fig. 1c). A displacement limit is set in the Z-plane, which prevents the barrier from sliding along the Z-axis. Rectangular mesh with an element size of 15 mm is considered.

III. RESULTS AND DISCUSSION

A. Static Analysis

The maximum von Mises equivalent stress resulting from the static loading is 911.8 MPa (Fig. 2a) close to the position where the load is applied on the halo. The maximum von Mises equivalent stress is less than the yield stress (1030 MPa) and hence the halo does not fail under these loading conditions. Although the largest stress occurs near the weld joint, since the stress is below the yield limit of the material failure of the joint does not occur and the joint is considered to be safe.

The total deformation of the halo is shown in Fig. 2b. The device experiences a maximum deformation of 2.2 mm which is below the 3 mm limit set by the FiA [5, 6], highlighting the superior properties of the material and the effectiveness of the simplified halo design as it withstands a 125 kN static load.

B. Dynamic Analysis

The evolution of von Mises equivalent stress in the halo during its impact against a steel barrier is shown in Fig. 3. The equivalent stress distribution in the steel barrier and the halo is shown in Fig. 4a. The evolution of von Mises equivalent stress and plastic strain with time are shown in Fig. 3d. The von Mises equivalent stress distribution in the halo before its failure is shown in Fig. 3a. A maximum von Mises equivalent stress of 1298 MPa is obtained at 2.4×10^{-4} s (Fig. 3d) and it occurs in the central pylon (Fig. 3a), i.e., the region of impact with the barrier. Fig. 3d shows that the equivalent stress decreases after the maximum value is reached. The stresses are relaxed due to the drastic increase in plastic strain from this point onward (Fig. 3d). The sudden decrease in the equivalent stress after 6×10^{-4} s is due to the complete failure of the halo, i.e., separation of the pylon from the U-section (Fig. 3b–c). The plastic strain remains constant after the failure of the halo. However, the equivalent stress still varies beyond this point as the broken pylon is still in contact with the barrier for the rest of the simulation (Fig. 4a).

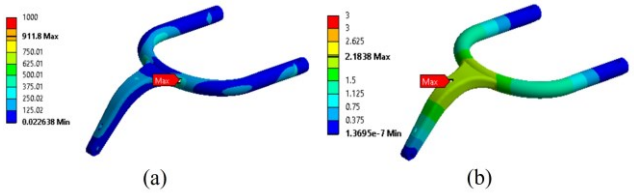

Fig. 2. Performance of the halo under static loading. (a) von Mises equivalent stress (MPa) and (b) total deformation (mm).

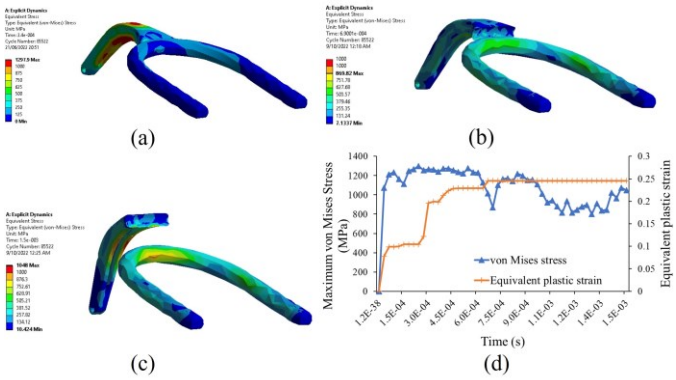

Fig. 3. von Mises equivalent stress in the halo during impact with a steel barrier at t = (a) 2.4×10^{-4} s, (b) 6.9×10^{-4} s, (c) 1.5×10^{-3} s. (d) Evolution of von Mises equivalent stress and equivalent plastic strain in the halo during the impact.

The equivalent stress is initially concentrated near the area of impact on the barrier and as time progresses, it is distributed over the entire barrier (Fig. 4a). The maximum equivalent stress obtained in the barrier is 3927 MPa, indicating failure of the steel barrier. The failure and breakage of the halo can be seen. The equivalent plastic strain, damage scalar (DAMAGEALL) and temperature distribution in the halo at the final instance of the loading, i.e., after breakage of the halo, are shown in Figs. 4b–d. The DAMAGEALL value of 0.314 (Fig. 4c) corresponds to the damage incurred by the central pylon and not to the entire halo assembly. Although separation of the central pylon from the tubular section can be seen in Fig. 4c, which would mean that a DAMAGEALL value of 1 would be expected, we do not see major damage to the individual components of the halo, e.g., central pylon, tubular section. Since the individual components of the halo were designed individually and joined to each other, ANSYS does not consider the entire structure as one single component. Therefore, ANSYS does not consider the separation between the tubular section and the pylon as damage. The maximum equivalent plastic strain, maximum damage, and maximum temperature (Figs. 4b–d) occur near the joint region of the pylon and the U-section depicting the importance of weld joints in deciding the safety of the halo impact protection device of F1 race cars.

IV. CONCLUSIONS

The performance of the halo impact protection device used in F1 race cars under static and dynamic loading conditions is studied using finite element analysis (FEA). The static loading

International Journal of Engineering Research & Technology (IJERT)
ISSN: 2278-0181
Volume 13, Issue 03 March 2024

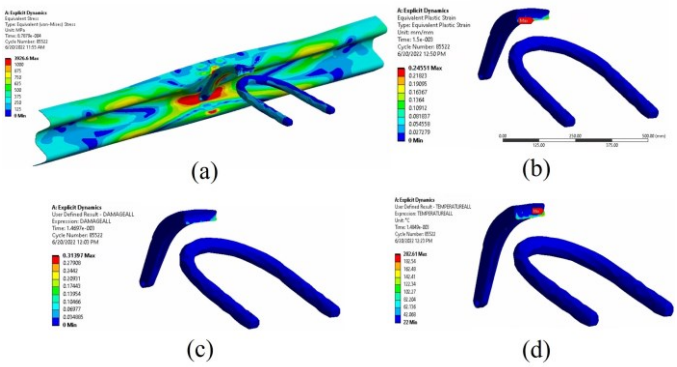

Fig. 4. (a) von Mises equivalent stress, (b) equivalent plastic strain, (c) damage scalar (DAMAGEALL) and (d) temperature in the halo during the final stages of its impact with a steel barrier.

analysis shows that the device can safely withstand a 125 kN static load as the maximum von Mises stress is less than the static yield strength and the maximum deformation is 2.2 mm, which is within the limit set by FiA.

FEA of the dynamic loading condition, i.e., impact of halo against a steel barrier, is performed by considering Johnson-Cook constitutive model. The results show that the maximum von Mises equivalent stress is concentrated in the central pylon where the impact occurs. Thereafter, the stress drops significantly due to the relaxation provided by plastic deformation and finally the halo device breaks, i.e., when the pylon detaches from the U-section of the halo. The maximum equivalent plastic strain, maximum damage and maximum temperature occur near the joint region of the pylon and the U-section. These results emphasize the essence of careful selection of the joining method and joining process parameters in deciding the failure of the halo impact protection device during F1 race car accidents.

Advanced modelling approaches, such as phase-field method [29-31] and molecular dynamics simulations [32,33], can be used in future to study the microstructure evolution and nanoscale phenomena during α–ω phase transformation in Ti-alloys under impact loadings.

ACKNOWLEDGMENT

This work made use of the computational facilities at Newcastle University.

REFERENCES

[1] FiA: F1 - WHY HALO IS THE BEST SOLUTION. www.fia.com/news/f1-why-halo-best-solution (2017). Accessed 17 May 2023.
[2] Richards, G.: FIA defends decision to enforce F1 halo cockpit protection device for 2018. The Guardian, 22 July 2017. https://www.theguardian.com/sport/2017/jul/22/formula-one-fia-defends-decision-halo-cockpit (2017). Accessed 17 May 2023.
[3] Galloway, J.: Romain Grosjean accident: Ross Brawn says Halo saved Haas driver's life. Sky Sports, 30 November 2020. https://www.skysports.com/f1/news/24219/12146618/romain-grosjean-accident-ross-brawn-says-halo-saved-haas-drivers-life (2020). Accessed 17 May 2023.
[4] Holding, J.: Zhou Guanyu credits halo after surviving British GP horror crash. BBC TopGear, 4 July 2022. www.topgear.com/car-news/formula-one/zhou-guanyu-credits-halo-after-surviving-british-gp-horror-crash (2022). Accessed 17 May 2023.
[5] F´ed´eration Internationale de l'Automobile: 2020 Formula 1 Technical Regulations. Issue 5, pp. 1–111 (2020).
[6] F´ed´eration Internationale de l'Automobile: Single-seater Additional Frontal Pro- tection - HALO. FIA Standard 8869-2018, pp. 1–19 (2019).
[7] Metar, M. and Attar, H.: Finite element analysis of F1 halo safety structure. Int. J. Res. Appl. Sci. Eng. Tech., 9, 1686–1689 (2021).
[8] Edmondson, L.: What is Halo and why is it being introduced in F1 for 2018?. ESPN, 20 July 2017. www.espn.co.uk/f1/story/ /id/20111099/what-halo-why-being-introduced-f1-2018.(2017). Accessed 17 May 2023.
[9] MacLeod, S.G., Errandonea, D., Cox, G.A., Cynn, H., Daisenberger, D., Finnegan, S.E., McMahon, M.I., Munro, K.A., Popescu, C. and Storm, C.V.: The phase diagram of Ti-6Al-4V at high-pressures and high-temperatures. J. Phys.: Condens. Matter 33, 154001–154001 (2021).
[10] Collings, E.W.: The Physical Metallurgy of Titanium Alloys. American Society for Metals, OH, USA (1984).
[11] MacLeod, S.G., Tegner, B.E., Cynn, H., Evans, W.J., Proctor, J.E., McMahon, M.I., Ackland, G.J.: Experimental and theoretical study of Ti-6Al-4V to 220 GPa. Phys. Rev. B 85, 224202–224202 (2012).
[12] Chesnut, G.N., Velisavljevic, N. Sanchez, L.: Shock compression of Condensed Matter. In: Elert M et al. (eds.) pp 27–30. AIP, New York (2007).
[13] Velisavljevic, N., Jacobsen, M.K. Vohra, Y.K.: Structural phase stability in nanocrystalline titanium to 161 GPa. Mater. Res. Exp. 1, 035044–035044 (2014).
[14] Sikka, S.K., Vohra, Y.K. Chidambaram, R.: Omega phase in materials. Prog. Mater. Sci. 27, 245–310 (1982).
[15] Singh, A.K.: The kinetics of pressure-induced polymorphic transformations. Bull. Mater. Sci. 5,3 219–230 (1983).
[16] Kutsar, A.R. German, V.N.: The investigation of the titanium structure after shock wave loading. In: Williams, J.C., Belov, A.F. (eds.) Titanium and Titanium Alloys. Vol.3, pp. 1633–1640. Springer, New York (1982).
[17] Autodesk® Inventor software.
[18] ANSYS® Academic Research Mechanical, Release 18.1.
[19] Hou, X., Liu, Z., Wang, B., Lv, W., Liang, X., Hua, Y.: Stress-strain curves and modified material constitutive model for Ti-6Al-4V over the wide ranges of strain rate and temperature. Mater. 11, 938–938 (2018).
[20] Murugesan, M., Jung, D.W.: Johnson Cook material and failure model parameters estimation of AISI-1045 medium carbon steel for metal forming applications. Mater. 12, 609–609 (2019).
[21] Huang, J., Guo, Y., Qin, D., Zhou, Z., Li, D., Li, Y.: Influence of stress triaxiality on the failure behavior of Ti-6Al-4V alloy under a broad range of strain rates. Theor. Appl. Fract. Mech. 97, 48–61 (2018).
[22] Wilson-Heid, A.E., Beese, A.M.: Fracture of laser powder bed fusion additively manufactured Ti–6Al–4V under multiaxial loading: Calibration and comparison of fracture models. Mater. Sci. Eng. A 761, 137967 (2019).
[23] Cherukara, A.: Study of the Halo Impact Protection System of Formula 1 cars: Material, Microstructure, Properties and Performance. BEng Thesis, Newcastle University, UK (2021).
[24] Yu, H., Li, W., Zou, H., Li, S., Zhai, T., Liu, L.: Study on non-isothermal transformation of Ti-6Al-4V in solution heating stage. Metals 9(9), 968–968 (2019).
[25] Galindo-Fernandez, M.A., Mumtaz, K., Rivera-Diaz-del-Castillo, P.E.J., Galindo- Nava, E.I., Ghadbeigi, H.: A microstructure sensitive model for deformation of Ti-6Al-4V describing cast-and-wrought and additive manufacturing morphologies. Mater. and Des. 160, 350–362 (2018).
[26] Jadhav, S., Powar, A., Patil, S., Supare, A., Farane, B., Singh, R.: Effect of volume fraction of alpha and transformed beta on the high cycle fatigue properties of bimodal Ti6Al4V alloy. IOP Conf. Series: Mater. Sci. Eng. 201, 012035–012035 (2017).
[27] Zafari, A., Xia, K.: High ductility in a fully martensitic microstructure: a paradox in a Ti alloy produced by selective laser melting. Mater. Res. Lett. 6(11), 627–633 (2018).
[28] Williams, J.C., Hickman, B.S., Marcus, H.L.: The effect of omega phase on the mechanical properties of titanium alloys. Metall. Trans. 2, 1913–1919 (1971).
[29] Yeddu, H.K., Lookman, T., Borgenstam, A., Ågren, J., Saxena, A.: Martensite formation in stainless steels under transient loading. Mater. Sci. Eng. A 594, 48–51 (2014).
[30] Brown, J., Yeddu, H.K.: Effect of hydrostatic pressure on the kinetics of alpha–omega phase transformation in zirconium. Modelling Simul. Mater. Sci. Eng. 30, 045008 (2022).
[31] Yeddu, H.K., Zong, H., Lookman, T.: Alpha - omega and omega - alpha phase transformations in zirconium under hydrostatic pressure: A 3D mesoscale study. Acta Mater. 102, 97-107 (2016).

International Journal of Engineering Research & Technology (IJERT)
ISSN: 2278-0181
Volume 13, Issue 03 March 2024

[32] Chen, J., Huo, D., Yeddu, H.K.: Molecular dynamics study of phase transformations in NiTi shape memory alloy embedded with precipitates. Mater. Res. Express 8, 106508 (2021).
[33] Chen, J., Yeddu, H.K.: Study of ageing and size effects in Nickel–Titanium shape memory alloy using molecular dynamics simulations. Phase Transit. 96:8, 596-606 (2023).
[34] Li, T., Zong, H.: Phase transformation mediated anomalous plasticity of titanium under severe loading conditions. Int. J. Mech. Sci. 231, 107799 (2023).